https://doi.org/10.3311/PPch.42481

Periodica Polytechnica Chemical Engineering

Highly Sensitive Hybrid Surface Plasmon Resonance Biosensor Utilizing Carbon Nanotube, Copper, Palladium and Black Phosphorus Layers

Hiba Bouandas[1], Rajeev Kumar[2], Lalit Garia[3], Mostefa Benhalilba[4*]

[1] Applied Optics Laboratory, Institute of Optics and Precision Mechanics, University Setif 1, Setif 19000, Algeria
[2] Department of Electronics and Communication, Engineering, Graphic Era (Deemed to be University), Dehradun, Uttarakhand 248001, India
[3] Department Electronics and Communication Engineering, BKIT Dwarahat, Uttarakhand 263653, India
[4] Film Device Fabrication-Characterization and Application FDFCA Research Group -USTOMB University, 31130 Oran, Algeria
* Corresponding author, e-mail: mostefa.benhalilba@univ-usto.dz

Received: 13 October 2025, Accepted: 27 January 2026, Published online: 20 February 2026

Abstract

In this work, a hybrid surface plasmon resonance sensor structure comprising carbon nanotube, copper, palladium and black phosphorus layer is presented for the detect of water salinity concentration. The angular interrogation method is used to evaluate key performance parameters such as sensitivity, detection accuracy, figure of merit (FoM) and penetration depth (PD). The Cu and Pd layer thicknesses are optimized to obtained the maximum sensitivity. The maximum sensitivity of 485.57 °/refractive index unit (RIU) and FoM of 122.92/RIU are obtained at thickness of 41 nm for Cu and 15 nm for PD layer. Moreover, the penetration depth of 140.45 nm and 143.28 nm are obtained for refractive indices of 1.3300 and 1.3369, respectively, corresponding to different water salinity. The suggested sensor has strong field penetration and high sensitivity due to the integration of cutting-edge materials and optimized design, which makes it appropriate for the practical detection of larger macromolecules in biosensing applications.

Keywords

surface plasmon resonance, sensitivity, detection accuracy, penetration depth

1 Introduction

Surface plasmon resonance (SPR) biosensor is becoming increasingly popular for detecting analytes like chemicals, biomolecules, bacteria and viruses [1–3]. SPR is an optical sensing method that is frequently used to detect molecular interactions in real time without the need for a label. Its foundation is the idea that when polarized light strikes at a particular angle, it generates surface plasmons (SPs), which are coherent oscillations of free electrons, at the interface between a metal (usually gold, silver) and a dielectric medium. When analytes bind to immobilized ligands, the refractive index (RI) changes close to the metal surface, which causes detectable shifts in the resonance angle ($\Delta\theta_{res}$). The ability to provide kinetic and affinity data, as well as its high sensitivity and quick response, has made SPR a potent tool in chemical and biological sensing. It is widely used for the detection of analytes, such as small molecules, proteins, nucleic acids, bacteria, and viruses, in pharmaceutical development, environmental monitoring, food safety and medical diagnostics. The two fundamental configurations utilized in prism-coupled SPR sensors are Otto and Kretschmann [4, 5]. While one prism face is fixed to the metal in the Kretschmann configuration, an air gap is created between the prism and metal in the Otto configuration. The Kretschmann configuration generates plasmons efficiently and is easy to implement, making it a good option for SPR sensing applications [4, 5]. Alterations in the sensing medium (SM) result in change in the resonance angle and change in the dip of the resonance curve. The prism-based sensor generates an evanescent wave when a transverse magnetic (TM), *p*-polarized light strikes the prism's single interface, passes through a thin layer of metal and generates the SP in the end at the metal-analyte boundary [6–8]. DNA hybridization, protein conformational studies, antibody characterization, cancer cell detection, and the identification of bacteria like pseudomonas and different viruses like COVID-19 and SARS are just a few of the real-time

Cite this article as: Bouandas, H., Kumar, R., Garia, L., Benhalilba, M. "Highly Sensitive Hybrid Surface Plasmon Resonance Biosensor Utilizing Carbon Nanotube, Copper, Palladium and Black Phosphorus Layers", Periodica Polytechnica Chemical Engineering, 2026. https://doi.org/10.3311/PPch.42481

applications that use the SPR sensing technique [9–12]. During the past three decades, SPR technology has been used to develop a number of well-known applications, including gas sensing, foodborne marker screening, environmental monitoring, disease diagnosis, and food safety. Plasmonic metals that can be utilized in the SPR sensor include Au, Ag, copper and aluminum [13]. These metallic elements meet the requirements of the free-electron criterion. Because Au has more merits than Ag, it is included in this study. Among its characteristics are increased stability, sensitivity, and resistance to corrosion. Ag, however, is less sensitive and oxidizes more readily. Design complexity arises from the need for extra layers of protection because other metals, such as Al and Cu, oxidize easily [14]. Several studies have previously reported the utilized of bimetallic-based SPR sensor structures, demonstrating improved plasmonic performance through the synergistic properties of two various metals. Bimetallic SPR sensors integrate two metals like Au–Ag, Au–Cu, Ag–Cu, or Au–Al in order to take advantage of their complementary plasmonic properties. These hybrid metal structures frequently exhibit improved chemical stability, sensitivity, tunable resonance behavior, and enhanced electric field confinement. Because of the two metals' synergy, researchers can get around some of the drawbacks of single-metal SPR sensors, like oxidation in Ag or reduced sensitivity in Au [15–17]. The performance of the biosensor is enhanced by the introduction of 2D materials above the metal layers mounted over the glass prism, which serve as a protective layer for the metal due to the reduced adsorbing capabilities of metal films. As technology has advanced, 2D materials are used in sensing applications. Graphene and other 2D materials are widely used in the SPR sensor. To increase the sensitivity of SPR, the scientific community has recently focused on designing a heterostructure of highly desirable 2D materials on a single chip. Different from their constituent materials, 2D-2D heterostructure alter their electrical and optical characteristics, making them ideal for enhancing SPR signals. An increase in the cost and complexity of the SPR device results from the difficulty of precisely stacking and aligning various 2D materials when creating such a heterostructure. Nonetheless, it is a tried-and-true method to increase the sensitivity of the SPR sensor by covering it with silicon. Many researchers have employed silicon in the past ten years without raising the price or complexity of the SPR sensor, which uses 2D nanomaterials to detect biomolecules. At the sensing interface, the TM field intensity is enhanced by this high RI dielectric material. Verma et al. utilized a silicon and graphene layer to create an SPR sensor [18]. The use of silicon between the graphene and Au layers greatly improves sensitivity. To get the maximum sensitivity, she enhanced the thickness of the silicon and Au layers and the number of graphene layers. Compared to other 2D materials like graphene and MoS_2, black phosphorus (BP), a layered two-dimensional semiconductor made of phosphorene sheets, has a special set of optical, electronic, and structural characteristics. BP's thickness-dependent bandgap (0.3–2.0 eV), strong light–matter interaction, and highly anisotropic in-plane permittivity make it especially appealing for plasmonic applications. BP helps to improve field localization at the metal–dielectric interface in SPR sensors, which results in increased sensitivity, a greater resonance angle shift and better detection performance. High-performance biosensing in chemical, environmental and biomedical applications is also made possible by BP's strong binding with biomolecules due to its large surface area and chemical reactivity. Consequently, BP-based SPR architectures have become a viable way to overcome the drawbacks of traditional metal-only sensors [19–21]. MXenes, which have the general formula $M_{n+1}X_nT_x$, are a growing class of 2D materials made of transition metal carbides, nitrides and carbonitrides. Their unique blend of high RI, metallic conductivity and customizable surface terminations result in powerful plasmonic properties that are especially useful for SPR sensing. According to recent reports, the sensitivity, figure of merit and biomolecule-binding efficiency of MXene-integrated SPR platforms have significantly improved. These benefits result from MXene's capacity to provide a large number of active sites for analyte adsorption, support localized surface plasmons and speed up charge transfer. As a result, MXene-based SPR sensors are receiving a lot of interest as viable substitutes for BP, MoS_2, and graphene in next-generation biosensing application [22, 23]. Ouyang et al. suggested using transition metal dichalcogenides (TMDs) and silicon on the Au layer in the SPR sensor at various wavelengths [24]. According to the results, the silicon layer significantly increases sensitivity. The results of an SPR sensor based on silicon and BlueP/MoS_2 have been proposed and analyzed by Srivastava et al. [25]. Comparing this sensor to the traditional SPR sensor, it was much more sensitive and could pick up even the smallest change in RI. To attach analytes and further improve sensitivity, BlueP/MoS_2 was employed as an interacting layer. In comparison to the traditional SPR sensor, the maximum sensitivity was attained 2–4 times higher. Pal et al. [26] showed an SPR biosensor based on Si-BP-TMD, which showed an improvement in sensitivity of

184.6 °/refractive index unit (RIU). The sensor's sensitivity is higher than that of a traditional SPR sensor. Recent developments in 2D-material-assisted and plasmonic SPR sensing show quick progress in improving surface selectivity, field confinement and sensitivity. A g-C_3N_4/chitosan nanocomposite-based SPR sensor has demonstrated high selectivity toward nitrite detection, highlighting the role of polymer–2D hybrids in surface functionalization and analyte adsorption [27]. Similarly, an AuNP@rGO-modified SPR platform has achieved notable improvement in plasmonic coupling for chemical detection, reporting sensitivity around 241 °/μM for melamine analysis in dairy matrices [28]. Nanomaterial integration has also helped fiber-optic SPR sensors. For instance, a graphene-oxide/chitosan-coated plasmonic fiber reported an ultrahigh sensitivity of 2315.2 nm/μM for amlodipine detection [3]. As demonstrated by recent innovations employing transition-metal compounds and emerging functional materials [29, 30], parallel developments in nanostructure-enhanced plasmonics show that alternative 2D materials and metal–dielectric composites continue to push performance boundaries. Further insights into nanoparticle-driven SPR modulation reveal that extinction, absorption, and resonance properties strongly depend on nanoscale parameters like particle size and concentration, underscoring the significance of precise thickness control in multilayer SPR structures [31]. In order to enhance optical confinement and nonlinear responses in plasmonic interfaces, the integration of sophisticated photonic and 2D materials has also been investigated, increasing the potential for next-generation SPR configurations [32]. The need for optimized multilayer architectures like the one suggested in this work is driven by the fact that material engineering, especially through 2D nanomaterials, bimetallic layers and nanocomposites, is essential to obtaining higher sensitivity, narrower resonance widths, and superior figure of merit in contemporary SPR sensors.

2 Proposed structure, refractive index, fabrication feasibility, theoretical modeling and performance matrices

2.1 Proposed sensor and fabrication feasibility

The suggested design is composed of six layers sensing layer, BK7 prism, CNT, Cu, Pd, and BP, as shown in Fig. 1. A multilayer SPR sensor integrated into the traditional Kretschmann prism configuration is depicted in the figure. After passing through a high-index BK7 glass prism, a *p*-polarized laser beam hits the metal stack at an incident angle that can be adjusted. A thin CNT layer is used

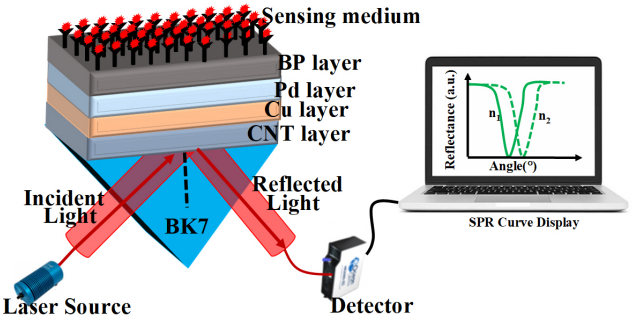

Fig. 1 Proposed SPR sensor

on the prism base first, followed by a Cu layer that facilitates surface-plasmon excitation, a Pd layer for adhesion and extra electric-field confinement, and a BP layer that comes into direct contact with the sample. Photons couple into collective electron oscillations in the Cu film when the laser angle meets the SPR condition, resulting in a dramatic drop in the intensity of reflected light. Following the selection of all materials, the performance parameters are measured, and the reflectance is estimated using the transfer matrix method (TMM) technique.

The refractive index of BK7 glass prism is 1.5151, it is employed as a coupling device. The second layer of CNT thin film of thickness 1 nm, then the third thin film of Cu, which is designed for a thickness between 35 and 65 nm and is utilized as the plasmonic metal. Pd, the fourth layer, is used to increase sensitivity even more. BP, the fifth layer, is used to boost sensitivity. The last layer serves as a water salinity medium for sensing. The materials used in the suggested sensor, along with their corresponding RIs and thicknesses, are listed in Table 1 [33–37].

2.2 Fabrication process

Fig. 2 shows the multilayered sensor structure fabrication on a BK7 prism substrate is made step-by-step. Using chemical vapor deposition (CVD) [38], a layer of carbon nanotubes is first deposited onto the BK7 prism. Excellent electrical conductivity and the capacity to improve

Table 1 RI of all materials with thickness for the proposed sensor

Materials	Thickness of layer	RI	Ref.
BK7 prism	Semi-infinite	1.5151	[33]
CNT	1 nm	1.5093 + 0.19851i	[34]
Cu	30-65 nm	0.0369 + 4.5393i	[13]
Pd	5-15 nm	0.034 + 3.1546i	[35]
BP	L × BP*	3.5 + 0.01i	[36]
Water salinity	-	1.3300 (0%) – 1.3369 (30%)	[37]

*L is the number of layers.

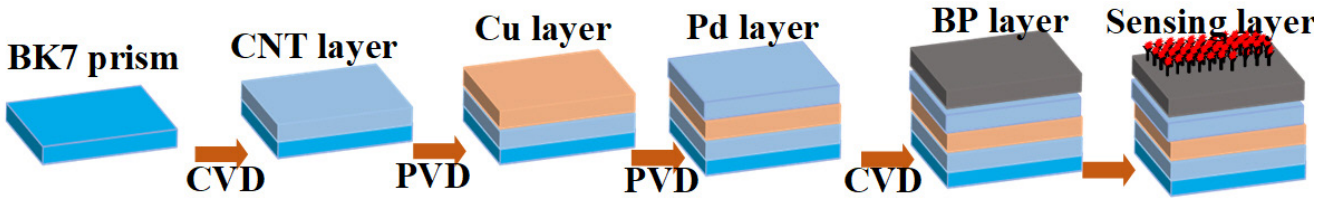

Fig. 2 Fabrication steps of the proposed sensor

electromagnetic field confinement are two well-known qualities of CNT. Physical vapor deposition (PVD) [39] is then used to deposit a Cu layer, which acts as a plasmonic material to facilitate surface plasmon polariton (SPP) excitation. Pd, another layer is added via PVD to increase the sensor's sensitivity and selectivity, especially for uses like biochemical or hydrogen detection. The performance of the sensor is then further enhanced by the CVD deposition of a BP layer, which provides anisotropic optical characteristics and a tunable bandgap [40]. Lastly, target analytes interact with the surface through a sensing layer that is applied on top. The resonance conditions of the SPPs are impacted by variations in the refractive index within this layer, allowing for extremely sensitive detection. This meticulously designed layered structure maximizes field enhancement and sensing capabilities by utilizing the distinct optical and plasmonic characteristics of each material. Stability, repeatability, and selectivity are among the promising properties of the suggested SPR sensor, which was built using a sequential layer-by-layer fabrication process that included a BK7 prism, CNT, Cu, Pd, BP and a sensing layer. By using strong materials with good chemical and thermal durability, like copper and palladium, the sensor's stability is largely maintained. Even though they are extremely sensitive, layers like CNT, Pd and BP could oxidize or degrade in the environment, which could compromise their long-term stability if they are not encapsulated or used in controlled settings. By ensuring consistent layer thickness and material quality across various sensor batches precise fabrication techniques like CVD and PVD improve repeatability. This structural uniformity has a direct impact on reproducible sensor responses. The functionalized sensing layer, which can be modified to target specific analytes with particular biomolecules or chemical receptors, is largely responsible for the sensor's selectivity. Furthermore, the distinct surface characteristics and high surface-to-volume ratios of CNT, Cu, Pd and BP layers enhance selectivity and sensitivity. An SPR sensor's optical performance is largely dependent on the thickness of its layers, and both increasing and decreasing thickness can have a substantial impact on resonance behavior and sensitivity. The plasmonic field weakens when the thickness of the metal layer (such as Cu) is increased beyond its ideal range because light penetration into the metal is decreased. This leads to a wider resonance curve and an increased FWHM, which ultimately reduces the sensitivity of the sensor. On the other hand, reducing the thickness of the metal improves plasmonic coupling and field confinement at the metal–dielectric interface, which sharpens the resonance and boosts sensitivity. However, if the metal gets too thin, it may lose continuity, resulting in an unstable and poor plasmonic response. Although sensitivity typically decreases due to weaker field enhancement, reducing the thickness of the 2D material reduces absorption and may slightly sharpen the resonance. In order to maximize sensitivity, minimize FWHM and guarantee stable resonance characteristics, the thicknesses of both metal and 2D material layers must be carefully optimized in order to achieve the best SPR performance. Overall, the SPR sensor is a strong candidate for accurate and dependable detection in a variety of sensing applications due to the combination of cutting-edge materials and precise fabrication techniques.

2.3 Mathematical modeling

The transfer matrix method (TMM) for the N-layer model has been used to analyze the performance parameter of the proposed structure for p-polarized incident light. Here, the multilayer proposed structure is shown in Fig. 1. The periodic stacking of multilayered structures is considered along the Z-axis. The TMM with the N-layer structure is used to measure the reflectivity of the reflected light. TMM is a straightforward, efficient method that doesn't call for approximation. According to the Z-axis, the dielectric constant ε_k, permittivity μ_k and refractive index n_k determine the thickness of the k^{th} layer, denoted as d_k. The suffix value of k^{th} ranges from 0 to N−1. Tangential components of the electric and magnetic fields for the first and N^{th} layer boundaries are represented by an U_1, U_{N-1}, V_1 and V_{N-1}, respectively. The component for the tangential field is $Z = Z_1 = 0$ at the first boundary and $Z = Z_{N-1}$ at the last. Using the TM approach, which is displayed below Eqs. (1)-(7), the reflectivity was determined [25].

$$\begin{bmatrix} U_1 \\ V_1 \end{bmatrix} = M \begin{bmatrix} U_{N-1} \\ V_{N-1} \end{bmatrix} \tag{1}$$

This is an illustration of the characteristic transfer matrix for *p*-polarized light in the composite multilayered structure.

$$M = \prod_{k=2}^{N-1} M_k \tag{2}$$

Where k^{th} layer matrix is expressed as follows.

$$M_k = \begin{bmatrix} \cos\beta_k & -\left(i\sin\beta_k\right)/q_k \\ -iq_k\sin\beta_k & \cos\beta_k \end{bmatrix} \tag{3}$$

The phase shift β_k and optical admittance q_k can be expressed as follows:

$$\begin{aligned} \beta_k &= \frac{2\pi}{\lambda} n_k \cos\theta_k \left(Z_k - Z_{k-1}\right) \\ &= \frac{2\pi}{\lambda} d_k \sqrt{\varepsilon_k - \left(n_1 \sin\theta_1\right)^2} \end{aligned} \tag{4}$$

$$q_k = \sqrt{\frac{\mu_k}{\varepsilon_k}} \cos\theta_k = \frac{\sqrt{\left(\varepsilon_k - n_1^2 \sin^2\theta_1\right)}}{\varepsilon_k} \tag{5}$$

Here λ is the wavelength and θ_1 is the *p*-polarized incident light. The following equation establishes the reflection coefficient r_p:

$$r_p = \frac{\left(M_{11} + M_{12}q_N\right)q_1 - \left(M_{21} + M_{22}q_N\right)}{\left(M_{11} + M_{12}q_N\right)q_1 + \left(M_{21} + M_{22}q_N\right)}, \tag{6}$$

where M_{11}-M_{22} are the characteristic matrix for the k^{th} layers. It is the part of M_k value.

And the reflection intensity R_p is measured by the following equation:

$$R_p = \left|r_p\right|^2 \tag{7}$$

2.4 Performance parameters

Estimating the sensitivity *S*, full width at half maximum (FWHM), detection accuracy (DA) and figure of merit (FoM) are a common method to evaluating the effectiveness of SPR sensors [13]. The change in the SM's RI, Δn_s determines the reflectance and causes a shift in the resonance angle, Δ_{res}. In an SPR sensor, the sensitivity depends on both the resonance angle shift $\Delta\theta_{res}$ and Δn_s, which are specified as [25]:

$$S = \frac{\Delta\theta_{res}}{\Delta n_s}\left(^\circ / \mathrm{RIU}\right) \tag{8}$$

The reflectance curve can also be used to calculate the FWHM. It can be computed as follows:

$$\mathrm{FWHM} = \theta_2 - \theta_1\left(^\circ\right) \tag{9}$$

The resonance angles at 50% reflectance, as determined by the resonance curve, are denoted by θ_1 and θ_2.

It is possible to determine DA as follow:

$$\mathrm{DA} = \frac{1}{\mathrm{FWHM}}\left(/^\circ\right)$$

The sensor's sensitivity and DA are multiplied to determine the FoM.

$$\mathrm{FoM} = S \times \mathrm{DA}\left(/\mathrm{RIU}\right) \tag{10}$$

3 Results and discussion

To improve sensitivity for the identification of different biomolecules, this work uses the advised SPR designs based on CNT/Cu/Pd/BP/analyzer with RI ranging from 1.3300 to 1.3369. The performance parameter was computed with COMSOL Multiphysics and MATLAB.

3.1 Performance parameter analysis of conventional SPR sensor (Structures: BK7/CNT/Cu/Pd/SM)

In this section, the performance metrics of various SPR sensor structures have been compared. For various Pd layer thicknesses, the graph shows how the suggested SPR sensor's sensitivity varies with Cu layer thickness, as shown in Fig. 3(a). It is clear that as Cu and Pd thickness increase, so does the sensitivity. Increasing the Cu layer from 30 nm to 60 nm results in a consistent increase in sensitivity for a fixed Pd thickness, suggesting that a thicker Cu layer improves surface plasmon excitation and propagation and, consequently, the sensor's performance. Additionally, the sensitivity increases with increasing Pd thickness at each Cu thickness. The whole Cu thickness range, the sensor with 15 nm Pd continuously demonstrates the highest sensitivity, whereas the sensor without Pd layer (0 nm) displays the lowest sensitivity. This pattern implies that a Pd layer greatly enhances the plasmonic response of the sensor, most likely as a result of Pd superior catalytic qualities and capacity to improve interactions with the analyte. Consequently, the combination of an appropriately thick Cu layer and a sufficient Pd layer leads to a significant improvement in SPR sensor sensitivity; the best performance in the range under investigation is obtained with a configuration of roughly 60 nm Cu and 15 nm Pd. As seen

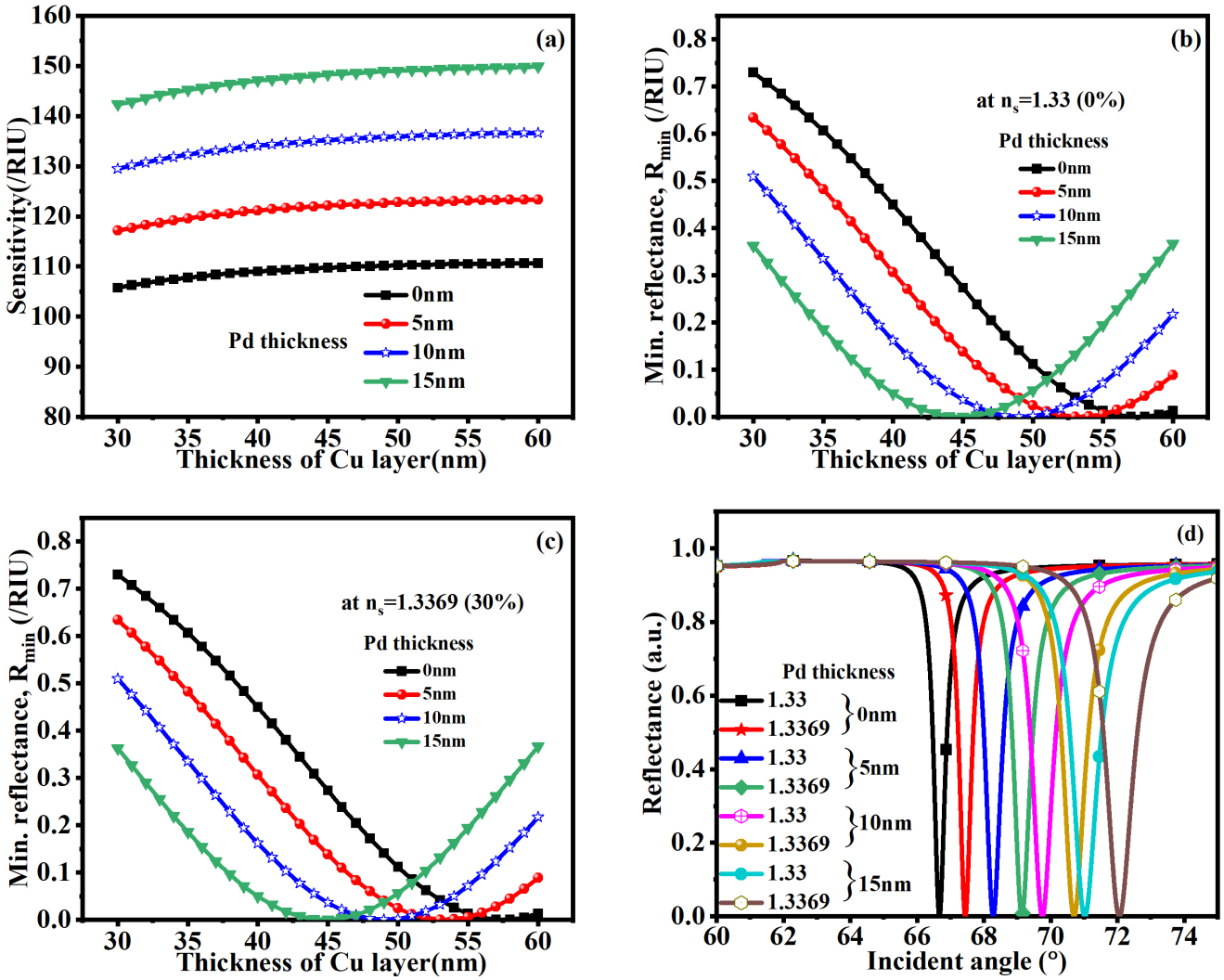

Fig. 3 (a) Sensitivity, (b) R_{min} at n_s = 1.3300, (c) R_{min} at n_s = 1.3369, (d) reflectance curve with various Pd thickness

in Figs. 3(b) and 3(c), the graph displays the change in the minimum reflectance R_{min} as a function of Cu thickness for various Pd thicknesses at refractive indices n_s = 1.3300 and 1.3369. When assessing the effectiveness of surface plasmon excitation in an SPR sensor, this plot is essential. As can be observed, the minimum reflectance initially falls as Cu thickness increases before starting to increase once more. The ideal Cu thickness for maximum plasmon resonance is shown by a clear minimum in the reflectance curve for all Pd thicknesses. Notably, a Pd layer greatly reduces the minimum reflectance, which results in a stronger plasmon resonance. At an ideal Cu thickness (45–50 nm), the sensor with 15 nm Pd has the lowest R_{min} among the curves, indicating the most effective SPR coupling. The black curve sensor, on the other hand, has a 0 nm Pd and maintains higher reflectance values throughout the whole Cu thickness range, suggesting less efficient plasmon excitation. This behavior demonstrates that in order to achieve strong SPR, both Pd and Cu thicknesses must be optimized. While a thicker layer (up to 15 nm) improves resonance by better facilitating the coupling between light and surface plasmons, a thinner Pd layer produces weaker resonance. Thus, the best results in terms of reducing R_{min} value and increasing plasmonic activity are obtained by combining a Pd thickness of 15 nm with a Cu thickness of about 45 nm. The performance of the SPR sensor for various Pd thicknesses (0, 5, 10, and 15 nm) under two refractive indices, 1.3300 and 1.3369, is depicted in the reflectance versus incident angle graph as shown in Fig. 3(d). Effective excitation of surface plasmons is indicated by a clear resonance dip, where the reflectance drops off dramatically with increasing Pd thickness. The resonance angle clearly shifts as the refractive index rises from 1.3300 to 1.3369, and this shift serves as the foundation for sensing in SPR systems. Interestingly, as Pd thickness increases, the angular shift becomes more noticeable.

Superior sensitivity and resolution are demonstrated by the sensor with 15 nm Pd, which exhibits the largest angular shift and the deepest and sharpest resonance dip. The sensor without a Pd layer (0 nm), on the other hand, exhibits a shallower and wider dip with less angular shift, indicating reduced sensitivity. The findings demonstrate that adding a Pd layer greatly improves the sensor's angular sensitivity and its capacity to pick up on minute variations in the SM. Therefore, by enabling more precise and dependable detection, a thicker Pd layer – especially around 15 nm – improves the SPR sensor's overall performance. Measured the performance parameters by the conventional sensor and displayed them in Table 2.

3.2 Investigate the effects of increasing the Pd layer (Structure: BK7/CNT/Cu/Pd/BPSM)

To enhance the CNT/Cu/Pd/BP-based sensor's performance parameter, a thorough analysis has been conducted. The suggested sensor's minimum reflectance after incident light should be zero in order to maximize its performance parameter. The R_{min} and maximum sensitivity are originally correlated with the thickness of the plasmon metals being optimized. Figs. 4(a)-(c) display the charts for R_{min} and sensitivity corresponding to different Cu and Pd thicknesses. The thickness of the Cu and Pd layers is chosen to maximize sensor performance, with R_{min} approaching 0 denoting the highest sensitivity. The sensitivity variation concerning optimal Cu thickness at different Pd layer thicknesses (5–15 nm) is displayed in Fig. 4(a). The sensitivity varies from 158.93 to 194.18 °/RIU, 214.34 to 290 °/RIU, and 350.98 to 485.57 °/RIU at Pd thicknesses of 5 nm, 10 nm, and 15 nm. As the Cu layer thickness grows, Fig. 4(a) demonstrates that the sensor's sensitivity rises as well. The sensitivity increases initially at a specific Cu layer thickness and subsequently decreases at a thickness of 15 nm for the Pd layer. At 41 nm Cu layer thickness, the maximum sensitivity of 485.57 °/RIU is attained with an impressive R_{min} value. At R_{min} values, the Cu and Pd layer thicknesses are 52 nm, 46 nm, and 41 nm, and 5 nm, 10 nm, and 15 nm, respectively. Yielding sensitivity values of 190.82 °/RIU, 270.65 °/RIU, and 485, 57 °/RIU. Table 3 contains the results of the computations for the various performance metrics. The R_{min} value changes for Cu thickness at different Pd layer thicknesses, with RI of SM 1.3300 and 1.3369, is displayed in Figs. 4(b) and 4(c). At a specific Cu layer thickness, the R_{min} value variation first decreases and subsequently increases in Figs. 4(b) and 4(c). We have determined the R_{min} values for the Cu layer at 52, 46, and 41 nm and the Pd layer at 5 nm, 10 nm, and 15 nm. The R_{min} values of 9.48×10^{-4} (a.u.), 1.2×10^{-5} (a.u.) and 1.686×10^{-3} (a.u.) are achieved at the same thickness. R_{min} values are obtained for different thicknesses of Cu and Pd at 1.33699 RI of SM, 2.33×10^{-4} (a.u.), 2.52×10^{-3} (a.u.), and 1.901×10^{-1} (a.u.). Fig. 4(c) illustrates that the Cu layer is 52 nm, 46 nm, and 41 nm thick, whereas the Pd layer is 5 nm, 10 nm, and 15 nm thick, respectively. The reflectance curve with different Cu and Pd layer thicknesses, 52 nm, 46 nm, and 41 nm, and 5 nm, 10 nm, and 15 nm, respectively at R_{min} values with RI of SM 1.3300 and 1.3369 is then displayed in Fig. 4(d). The resonance angle $\Delta\theta_{res}$ changes by 1.33°, 1.89°, and 3.39° at the same thickness. The FWHM rose in tandem with the Pd layer thickness. Table 3 shows the computed performance metrics, including FWHM, DA and FoM, at R_{min} values. Cu and Pd layers with thicknesses of 41 nm and 15 nm, respectively, yield the highest sensitivity of 485.57 °/RIU.

3.3 Investigate the effects of increasing the BP (L × 0.53 nm) layer

Increasing the BP layer's thickness (L × 0.53 nm) in a multilayer SPR sensor has several effects on the optical characteristics and performance metrics of the sensor. BP is extremely anisotropic and has a comparatively high RI. The effective RI of the sensor structure rises with the number of BP layers added. Since momentum matching between light waves and surface plasmon waves (SPWs) necessitates a greater angle of reflection, this increased RI causes the resonance angle to move to higher angles. The Ag layer's thickness affects BP's capacity to improve sensitivity and field confinement. We measured the

Table 2 Measure the performance parameters at R_{min} value

Cu thickness (nm)	S (°/RIU)	R_{min} (a.u.) at n_s = 1.3300	R_{min} (a.u.) at n_s = 1.3369	FWHM (°) at n_s = 1.3300	DA (1/°) at n_s = 1.3300	FoM (1/RIU) at n_s = 1.3300
57	110.57	5.1×10^{-4}	5.4×10^{-4}	0.43	2.32	257.15
53	122.95	2.9×10^{-4}	2.6×10^{-4}	0.59	1.69	208.39
49	135.82	2.8×10^{-5}	7.4×10^{-6}	0.77	1.29	176.39
45	148.28	6.1×10^{-5}	1.5×10^{-4}	0.96	1.04	154.45

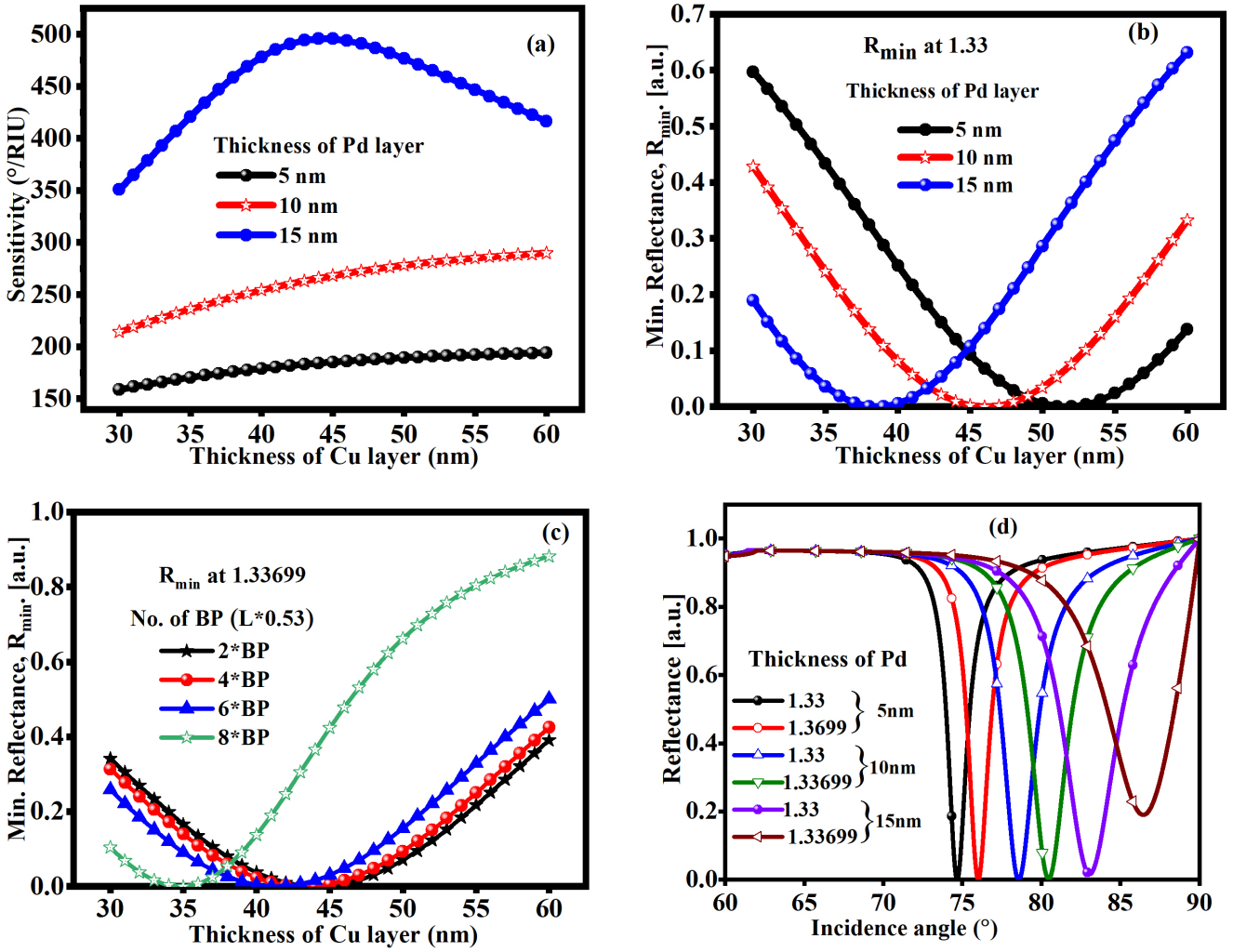

Fig. 4 (a) Sensitivity vs Cu thickness at various Pd thicknesses (b) R_{min} at n_s = 1.3300 RI of SM, (c) R_{min} at n_s = 1.3369 RI of SM, and (d) reflectance curve at various thicknesses of Cu and Pd

Table 3 Measured performance parameters for different Cu and Pd thicknesses at R_{min} with a conventional sensor with 1 nm of CNT thickness

Cu Thickness (nm)	Pd Thickness (nm)	S (°/RIU)	R_{min} (a.u.) at n_s = 1.3300	R_{min} (a.u.) at n_s = 1.3369	FWHM (°)	DA (1/°)	FoM (1/RIU)
52	5	190.82	9.4×10^{-5}	2.3×10^{-4}	1.46	0.68	130.69
46	10	270.65	1.2×10^{-5}	2.5×10^{-3}	2.44	0.40	110.92
41	15	485.57	1.6×10^{-3}	1.9×10^{-1}	3.95	0..25	122.92

performance characteristics in the suggested structure by increasing the BP (L = 2, 4, 6 and 8) layer. The results are shown graphically in Fig. 5. As the Cu layer thickness increases, we plot the sensitivity at the same BP layer thickness, as illustrated in Fig. 5(a). 158.03 to 170.65 °/RIU, 182.05 to 205.24 °/RIU, 225.49 to 280.08 °/RIU, and 350.98 to 485.57 °/RIU are the ranges of the sensitivity, respectively. As a result, with increasing BP and Cu layer thickness and BP layers, the SPR sensor becomes more sensitive because these materials enhance light-matter interactions, plasmonic field confinement, and coupling efficiency. The R_{min} value is displayed in Figs. 5(b) and 5(c) at different thicknesses of Cu (45 nm, 43 nm, 41 nm and 40 nm) and BP (L = 2, 4, 6, and 8) layers. The thickness of each layer is adjusted to enhance sensitivity while balancing optical losses and stability. The corresponding resonance angles at the same thickness are 72.79°, 75.06°, 78.11°, 83.05° (at n_s = 1.3300) and 73.97°, 76.44°, 79.92° and 86.44° (at n_s = 1.3369). The $\Delta\theta_{res}$ of 0.74°, 1.05° and 2.08° are obtained at the same resonance angle. Sensitivities of 167.95 °/RIU, 198.60 °/RIU, 258.44 °/RIU and 485.57 °/RIU are attained at the same $\Delta\theta_{res}$. Fig. 5(d) then shows the

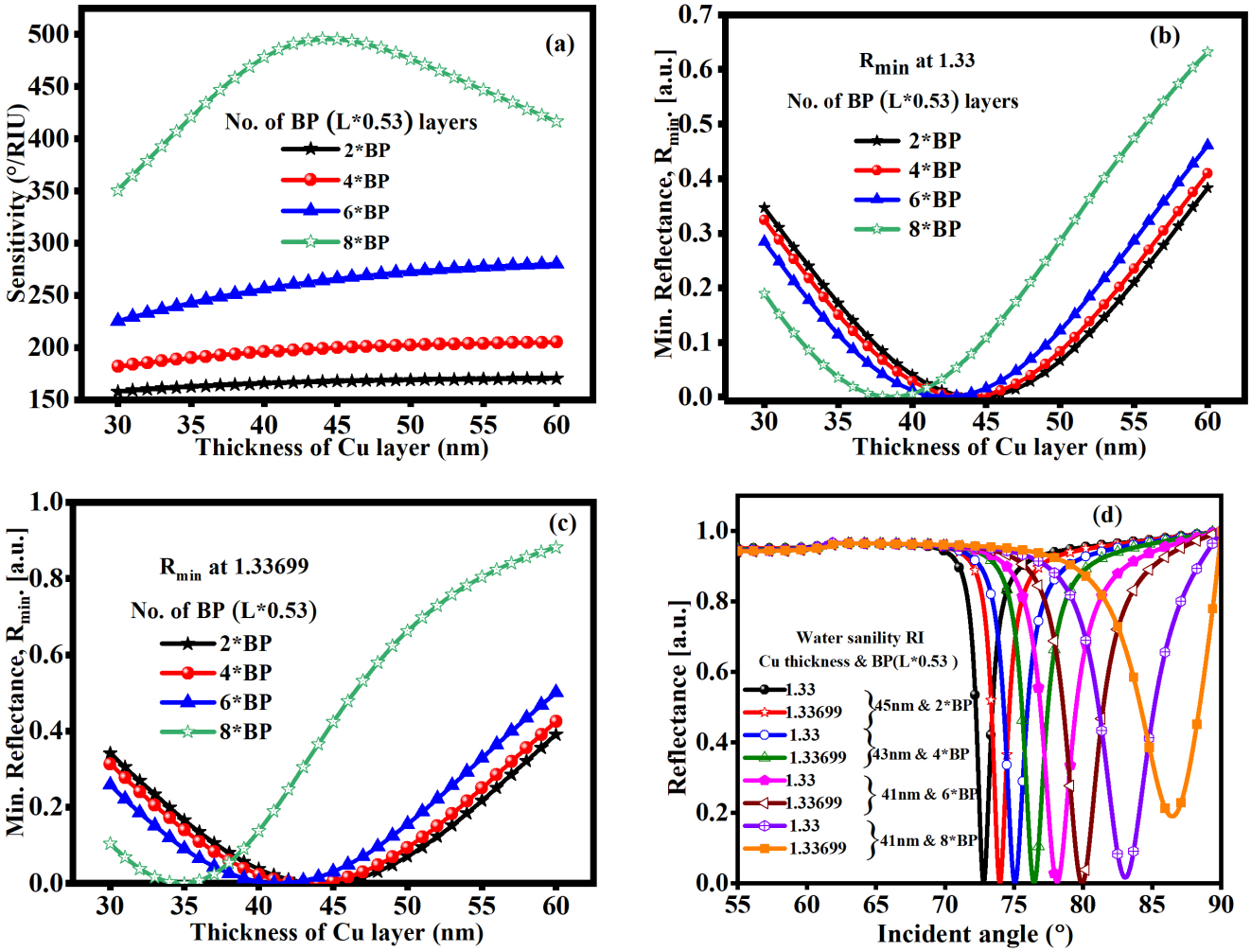

Fig. 5 (a) Sensitivity vs Cu thickness at various BP thickness; (b) R_{min} at n_s = 1.3300 RI of SM; (c) R_{min} at n_s = 1.3369 RI of SM and (d) reflectance curve at various thicknesses of Cu and BP

reflectance curve for R_{min} values with RI of SM 1.3300 and 1.3369 for various Cu and BP layer thicknesses of 45 nm, 43 nm, 41 nm and 41 nm, and 2 nm, 4 nm, 6 nm and 8 nm, respectively. At the same thickness, the resonance angle $\Delta\theta_{res}$ varies by 1.17°, 1.38°, 1.80° and 3.39°. The FWHM increased as the thickness of the Pd layer increased. The calculated performance measures, such as FWHM, DA and FoM, at R_{min} values are displayed in Table 4. Additionally, the sensitivity attained by this optimized configuration (Cu 41 nm and 8 × BP layers) is noticeably higher at 485.57 °/RIU, and the FWHM is noticeably higher than that of the traditional Cu-based SPR sensor.

3.4 Field analysis by the proposed sensor

The graph illustrates how the normalized electric field across a multilayer SPR sensor structure changes with the distance between the sensing medium and the BK7 prism as shown in Fig. 6. It also shows how different RIs

Table 4 Measured performance parameters for different Cu and BP thicknesses at R_{min} with conventional sensor with 1 nm and 15 nm of CNT and Pd thickness, respectively

Cu thickness (nm)	No. of BP layer	S (°/RIU)	R_{min} (a.u.) at n_s =1.3300	R_{min} at n_s =1.3369	FWHM (°)	DA (1/RIU)	FoM (1/°)
45	2	167.95	8.8×10^{-4}	0.0015	1.17	0.854	143.54
43	4	198.60	9.7×10^{-4}	9.73×10^{-4}	1.67	0.598	118.92
41	6	258.44	0.0040	2.80×10^{-4}	2.5	0.4	103.37
41	8	485.57	0.0168	0.1901	3.95	0..25	122.92

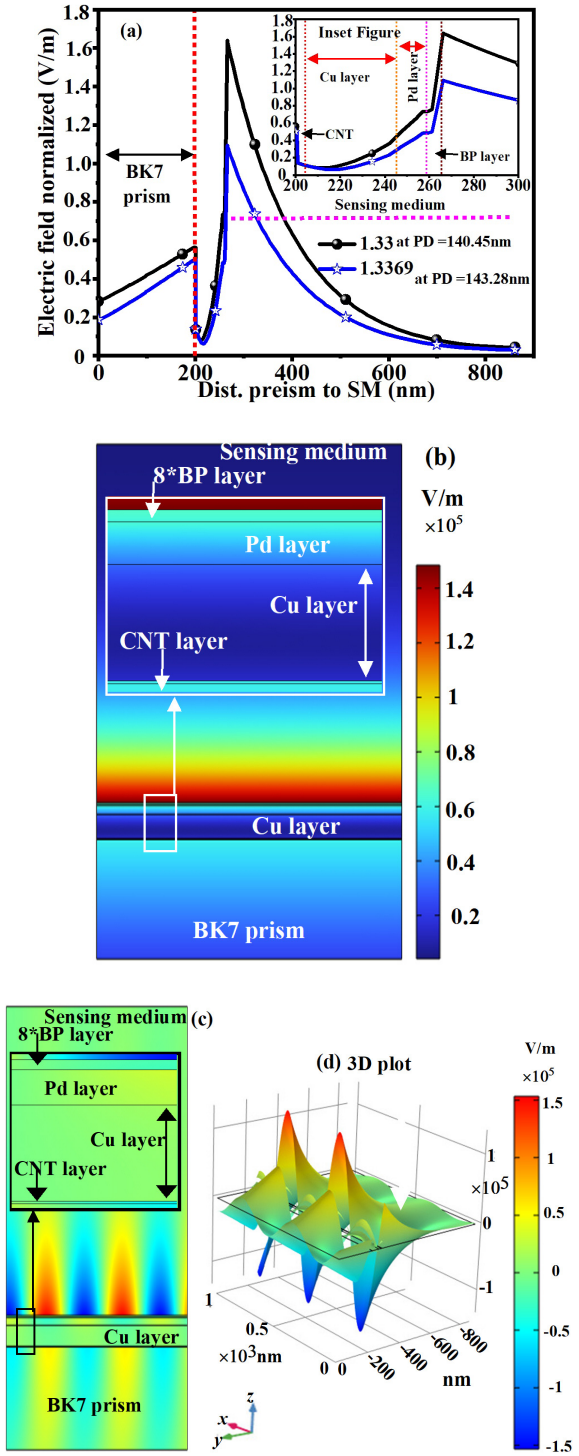

Fig. 6 (a) Electric field normalized with respect to the maximum field amplitude, (b) electric field distribution, (c) 2D plot of SPP mode (d) 3D plot of SPP mode with proposed structure

affect the penetration depth (PD) and intensity of the field. Electric field norm values are represented by two curves for refractive indices n_s = 1.3300 (black) and n_s = 1.3369 (blue), which correspond to varying salinity concentrations in the water. Near the BP-dielectric interface, a sharp peak in the electric field is seen, signifying strong plasmonic excitation – a crucial component in improving sensor sensitivity. The ability of the sensor to pick up on minute changes in the RI of SM is confirmed by the slight shift and magnitude decrease of the peak field with increasing refractive index. A detailed view of the electric field distribution across the CNT, Cu, Pd and BP layers is shown in the inset figure of Fig. 6(a), which also shows that the Pd and BP layers dramatically contribute to field confinement and enhancement. The utility of the multilayer design in optimizing the detection of salinity in water through enhanced plasmonic resonance close to the active sensing region and maximizing SPR sensitivity is confirmed by this electric field analysis. The PD of 140.45 nm and 143.28 nm is obtained with RI of 1.3300 and 1.3369. When an external light source excites the structure, the color map shows how the electric field intensity is distributed throughout the structure, as shown in Fig. 6(b). The Cu and CNT layer interfaces, as well as the locations of the upper Cu and Pd layers, are where the strongest field intensity (highlighted in red) is concentrated. These hot spots signify the excitation of surface plasmon polaritons, which are strongly confined electromagnetic waves produced at the metal-dielectric interface when light and electron oscillations are coupled. Surface plasmon polaritons are electromagnetic waves that are closely coupled to collective oscillations of the free electrons in a metal and move along the interface between a BP and a dielectric (non-conducting) material, as shown in Fig. 6(c). Fig. 6(d) shows the 3D plot of the SPP mode. The interaction between incident light and the free electrons at the BP surface causes oscillations that produce confined electromagnetic fields along the interface, giving rise to these waves.

Table 5 displays a comparison of the suggested sensor's sensitivity performance with earlier research [40–43]. The suggested work clearly achieves the highest sensitivity.

Table 5 Comparison of the sensitivity performance with existing published work

Authors and Ref.	Sensitivity (°/RIU)	Years
Kumar et al. [40]	304.47	2021
Yadav et al. [41]	288.86	2023
Ahmed et al. [42]	409.26	2025
Uniyal et al. [43]	263.57	2025
Proposed work	485.47	-

4 Conclusion

In the proposed work, the Pd-BP-based SPR sensor is theoretically designed and analyzed for the detection of water salinity concentration. By adjusting the thickness of the Cu, Pd and BP layers, the results are optimized to yield better results. Because of the higher FWHM, a Cu layer thickness of 41 nm is found to be able to provide the highest sensitivity. By optimizing the Cu (41 nm) and Pd (15 nm) layer thicknesses with 8*BP layer, the proposed structure achieved a maximum sensitivity of 485.57°/RIU and a FoM of 122.92/RIU, outperforming many conventional plasmonic structure. Moreover, calculated PD of 140.45 nm and 143.28 nm for RIs 1.330–1.33699 confirm the sensor's capability to detect larger macromolecules due to deeper evanescent-wave interaction. Overall, the suggested hybrid architecture shows great promise for extremely sensitive, stable, and selective refractive-index sensing, with potential uses in chemical analysis, biomedical diagnostics, and environmental monitoring.

References

[1] Kumar, R., Pandey, V. K., Alam, J., Garia, S., Singh, S. "Detection of cortisol using long range surface plasmon resonance sensor with enhance figure of merit", Microchemical Journal, 209, 112696, 2025. https://doi.org/10.1016/j.microc.2025.112696

[2] Ashrafi, T. M. S., Mohanty, G. "Surface Plasmon Resonance Sensors: A Critical Review of Recent Advances, Market Analysis, and Future Directions", Plasmonics, 20(8), pp. 6825–6845, 2025. https://doi.org/10.1007/s11468-024-02740-4

[3] Shakya, A. K., Ramola, A., Singh, S., Vidyarthi, A. "Optimized Design of Plasmonic Biosensor for Cancer Detection: Core Configuration and Nobel Material Coating Innovation", Plasmonics, 20(4), pp. 1789–1810, 2025. https://doi.org/10.1007/s11468-024-02400-7

[4] Otto, A. "Excitation of Nonradiative Surface Plasma Waves in Silver by the Method of Frustrated Total Reflection", Zeitschrift für Physik A Hadrons and nuclei, 216(4), pp. 398–410, 1968. https://doi.org/10.1007/BF01391532

[5] Kretschmann, E., Raether, H. "Notizen: Radiative Decay of Non Radiative Surface Plasmons Excited by Light", Zeitschrift für Naturforschung A, 23(12), pp. 2135–2136, 1968. https://doi.org/10.1515/zna-1968-1247

[6] Mishra, A. K., Mishra, S. K. "Gas Sensing in Kretschmann Configuration Utilizing Bi-Metallic Layer of Rhodium-Silver in Visible Region", Sensors and Actuators B: Chemical, 237, pp. 969–973, 2016. https://doi.org/10.1016/j.snb.2016.07.041

[7] Karki, B., Uniyal, A., Srivastava, G., Pal, A. "Black Phosphorous and Cytop Nanofilm-Based Long-Range SPR Sensor with Enhanced Quality Factor", Journal of Sensors, 2023, 2102915, 2023. https://doi.org/10.1155/2023/2102915

[8] Homola, J. "Surface Plasmon Resonance Sensors for Detection of Chemical and Biological Species", Chemical Reviews, 108(2), pp. 462–493, 2008. https://doi.org/10.1021/cr068107d

[9] Gumaih, H. S., Mollah, M. A., Adam, Y. S., Almawgani, A. H. M. "Prism Based Surface Plasmon Resonance Sensor Using Ag/$BaTiO_3$/BP Layers for Cancer Detection", Plasmonics, 20(6), pp. 3997–4006, 2025. https://doi.org/10.1007/s11468-024-02600-1

[10] Kumar, S., Yadav, A., Kumar, S., Malomed, B. A. "Design and Simulation of SPR Sensors by Employing Silicon and Silicon-Nitride With Mono and Bimetal Layers for Sensitivity Enhancement", IEEE Sensors Journal, 24(6), pp. 7671–7680, 2024. https://doi.org/10.1109/JSEN.2024.3355766

[11] Taya, S. A., Daher, M. G., Almawgani, A. H. M., Hindi, A. T., Zyoud, S. H., Colak, I. "Detection of Virus SARS-CoV-2 Using a Surface Plasmon Resonance Device Based on $BiFeO_3$-Graphene Layers", Plasmonics, 18(4), pp. 1441–1448, 2023. https://doi.org/10.1007/s11468-023-01867-0

[12] Karki, B., Pal, A., Sarkar, P., Yadav, R. B., Dhiman, G., Muduli, A. "Detection of Chikungunya Virus Using Tantalum Diselenide ($TaSe_2$)-Based Surface Plasmon Resonance Biosensor", Plasmonics, 19(5), pp. 2463–2472, 2024. https://doi.org/10.1007/s11468-023-02169-1

[13] Kumar, R., Pal, S., Prajapati, Y. K., Kumar, S., Saini, J. P. "Sensitivity Improvement of a MXene- Immobilized SPR Sensor With Ga-Doped-ZnO for Biomolecules Detection", IEEE Sensors Journal, 22(7), pp. 6536–6543, 2022. https://doi.org/10.1109/JSEN.2022.3154099

[14] Han, L., He, X., Ge, L., Huang, T., Ding, H., Wu, C. "Comprehensive Study of SPR Biosensor Performance Based on Metal-ITO-Graphene/TMDC Hybrid Multilayer", Plasmonics, 14(6), pp. 2021–2030, 2019. https://doi.org/10.1007/s11468-019-01004-w

[15] Houari, F., El Barghouti, M., Mir, A., Akjouj, A. "Nanosensors Based on Bimetallic Plasmonic Layer and Black Phosphorus: Application to Urine Glucose Detection", Sensors, 24(15), 5058, 2024. https://doi.org/10.3390/s24155058

[16] Kumar, R., Pal, S., Pal, N., Saini, J. P., Prajapati, Y. K. "Performance Evaluation of Bimetallic Surface Plasmon Resonance Sensor Based on $Ti_3C_2T_x$ (MXene)", In: Dhawan, A., Tripathi, V. S., Arya, K. V., Naik, K. (eds.) Recent Trends in Electronics and Communication: Select Proceedings of VCAS 2020, Springer Singapore, 2022, pp. 13–25. ISBN 978-981-16-2761-3 https://doi.org/10.1007/978-981-16-2761-3_2

[17] Maheswari, P., Ravi, V., Rajesh, K. B., Rahman, S. M. H., Jha, R. "High Performance SPR Biosensor Using Cu-Pt Bimetallic 2023. Layers and 2D Materials", Digest Journal of Nanomaterials and Biostructures, 18(1), pp. 221–234, 2023. https://doi.org/10.15251/DJNB.2023.181.221

[18] Verma, R., Gupta, B. D., Jha, R. "Sensitivity Enhancement of a Surface Plasmon Resonance Based Biomolecules Sensor Using Graphene and Silicon Layers", Sensors and Actuators B: Chemical, 160(1), pp. 623–631, 2011. https://doi.org/10.1016/j.snb.2011.08.039

[19] Kitada, S., Shimizu, N., Hossain, M. Z. "Safe and Fast Synthesis of Black Phosphorus and Its Purification", ACS Omega, 5(20), pp. 11389–11393, 2020. https://doi.org/10.1021/acsomega.0c00404

[20] Eswaraiah, V., Zeng, Q., Long, Y., Liu, Z. "Black Phosphorus Nanosheets: Synthesis, Characterization and Applications", Small, 12(26), pp. 3480–3502, 2016. https://doi.org/10.1002/smll.201600032

[21] Zeng, Y., Guo, Z. "Synthesis and Stabilization of Black Phosphorus and Phosphorene: Recent Progress and Perspectives", iScience, 24(10), 103116, 2021. https://doi.org/10.1016/j.isci.2021.103116

[22] Wu, Q., Li, N., Wang, Y., Liu, Y., Xu, Y., ..., Cui, X. "A 2D Transition Metal Carbide MXene-Based SPR Biosensor for Ultrasensitive Carcinoembryonic Antigen Detection", Biosensors and Bioelectronics, 144, 111697, 2019. https://doi.org/10.1016/j.bios.2019.111697

[23] Li, X., Ran, F., Yang, F., Long, J., Shao, L. "Advances in MXene Films: Synthesis, Assembly, and Applications", Transactions of Tianjin University, 27(3), pp. 217–247, 2021. https://doi.org/10.1007/s12209-021-00282-y

[24] Ouyang, Q., Zeng, S., Jiang, L., Hong, L., Xu, G., ..., Yong, K.-Y. "Sensitivity Enhancement of Transition Metal Dichalcogenides/ Silicon Nanostructure-Based Surface Plasmon Resonance Biosensor", Scientific Reports, 6(1), 28190, 2016. https://doi.org/10.1038/srep28190

[25] Srivastava, A., Prajapati, Y. K. "Performance Analysis of Silicon and Blue Phosphorene/MoS_2 Hetero-Structure Based SPR Sensor", Photonic Sensors, 9(3), pp. 284–292, 2019. https://doi.org/10.1007/s13320-019-0533-1

[26] Pal, S., Verma, A., Saini, J. P., Prajapati, Y. K. "Sensitivity Enhancement Using Silicon-Black Phosphorus-TDMC Coated Surface Plasmon Resonance Biosensor", IET Optoelectronics, 13(4), pp. 196–201, 2019. https://doi.org/10.1049/iet-opt.2018.5023

[27] Nasiri, H., Baheri-Fard, M., Abbasian, K., Khodaei, H., Alipour-Banaei, H. "Nitrite Detection in Food Samples by Surface Plasmon Resonance in Graphitic-Carbon Nitride/Chitosan Nanocomposite", Microchemical Journal, 214, 114071, 2025. https://doi.org/10.1016/j.microc.2025.114071

[28] Nasiri, H., Asl, E. S., Nilghaz, A., Kiani, G., Baheri-Fard, M. "Fabrication of AuNP@ RGO Nanocomposite for Melamine Detection in Dairy Products by Surface Plasmon Resonance", Optics & Laser Technology, 192, 113906, 2025. https://doi.org/10.1016/j.optlastec.2025.113906

[29] Bigbaghlou, R. G., Salahandish, M., Nasiri, H., Hashemzadeh, E., Pourziad, A. "Enhancing Wave Detection with Advanced Plasmonic Metamaterial Absorbers for Sensing Applications", Plasmonics, 20(9), pp. 7839–7849, 2025. https://doi.org/10.1007/s11468-024-02704-8

[30] Nasiri, H., Abbasian, K., Nilghaz, A. "Nitrite Detection with Trapping in RGO/Fe_2O_3 Composite Based on Surface Plasmon Resonance", Inorganic Chemistry Communication, 176, 114327, 2025. https://doi.org/10.1016/j.inoche.2025.114327

[31] Nasiri, H., Salahandish, M., Sharifi, H., Mohammadzadehasl, N. "Dependence of Extinction Cross-Section, Absorption and Surface Plasmon Resonance of Nanoparticle Surface Size and Concentration of Silica@ Gold Nanoparticles", Biomedical Materials & Devices, 3(2), pp. 1501–1508, 2025. https://doi.org/10.1007/s44174-024-00272-3

[32] Nasiri, H., Abbasian, K. "Surface Plasmon Resonance Detection of Anti-Cancer Drug Flutamide by Graphitic Carbon Nitride/Chitosan Nanocomposite", Scientific Reports, 15(1), 2278, 2025. https://doi.org/10.1038/s41598-025-86665-w

[33] Jha, R., Sharma, A. K. "Chalcogenide Glass Prism Based SPR Sensor with Ag-Au Bimetallic Nanoparticle Alloy in Infrared Wavelength Region", Journal of Optics A: Pure and Applied Optics, 11(4), 045502, 2009. https://doi.org/10.1088/1464-4258/11/4/045502

[34] Uniyal, A., Srivastava, G., Sarkar, P., Kumar, M., Singh, S., Taya, S. A., Muduli, A., Pal, A. "Fluorinated Graphene and CNT-Based Surface Plasmon Resonance Sensor for Detecting the Viral Particles of SARS-CoV-2", Physica B: Condensed Matter, 669, 415282, 2023. https://doi.org/10.1016/j.physb.2023.415282

[35] Bouandas, H., Slimani, Y., Alanazi, F. K., Fatmi, M., Chihi, T., Djemli, A. "Detection of Tuberculosis Using Palladium -Tantalum Diselenide (Pd-$TaSe_2$) Bases SPR Biosensor", Journal of Optics, 54(5), pp. 3649–3656, 2025. https://doi.org/10.1007/s12596-024-02088-2

[36] Srivastava, A., Verma, A., Das, R., Prajapati, Y. K. "A Theoretical Approach to Improve the Performance of SPR Biosensor Using MXene and Black Phosphorus", Optik, 203, 163430, 2020. https://doi.org/10.1016/j.ijleo.2019.163430

[37] Kumar, R., Singh, S., Garia, L., Chaudhary, B., Singh, M. K., Kumar, S. "A Numerical Analysis for the Detection of Water Salinity Concentration Using Long-Range Surface Plasmon Resonance Biosensor with TMDCs-Teflon/Cytop", IEEE Transactions on Plasma Science, 52(8), pp. 3136–3144, 2024. https://doi.org/10.1109/TPS.2024.3471636

[38] Nangare, S., Patil, P. "Black Phosphorus Nanostructure Based Highly Sensitive and Selective Surface Plasmon Resonance Sensor for Biological and Chemical Sensing: A Review", Critical Reviews in Analytical Chemistry, 53(1), pp. 1–26, 2023. https://doi.org/10.1080/10408347.2021.1927669

[39] Karki, B., Salah, N. H., Srivastava, G., Muduli, A., Yadav, R. B. "A Simulation Study for Dengue Virus Detection Using Surface Plasmon Resonance Sensor Heterostructure of Silver, Barium Titanate, and Cerium Oxide", Plasmonics, 18(6), pp. 2031–2040, 2023. https://doi.org/10.1007/s11468-023-01907-9

[40] Kumar, R., Pal, S., Pal, N., Mishra, V., Prajapati, Y. K. "High-Performance Bimetallic Surface Plasmon Resonance Biochemical Sensor Using a Black Phosphorus–MXene Hybrid Structure", Applied Physics A, 127(4), 259, 2021. https://doi.org/10.1007/s00339-021-04408-w

[41] Yadav, A., Mishra, M., Tripathy, S. K., Kumar, A., Singh, O. P., Sharan, P. "Improved Surface Plasmon Effect in Ag-Based SPR Biosensor with Graphene and WS_2: An Approach Towards Low Cost Urine-Glucose Detection", Plasmonics, 18(6), pp. 2273–2283, 2023. https://doi.org/10.1007/s11468-023-01945-3

[42] Ahmed, T., Hosain, M. K., Kouzani, A. Z. "Highly Sensitive SPR Sensor Employing Zinc Selenide, Silver Nanocomposite, and Lead Titanate for the Detection of Cancer Cells", Microchimica Acta, 192, 203, 2025. https://doi.org/10.1007/s00604-024-06867-3

[43] Uniyal, A., Pal, A., Ansari, G., Chauhan, B. "Numerical Simulation of InP and MXene-Based SPR Sensor for Different Cancerous Cells Detection", Cell Biochemistry and Biophysics, 83(3), pp. 2895–2908, 2025. https://doi.org/10.1007/s12013-025-01675-9